Materials Advances

ROYAL SOCIETY OF CHEMISTRY

PAPER

View Article Online
View Journal | View Issue

Cite this: *Mater. Adv.*, 2025, 6, 4313

Influence of amino silane-modified nanocellulose on the physico-chemical and mechanical properties of alginate films†

Shenbagaraman Akshaya[ab] and A. Joseph Nathanael *[b]

Received 21st March 2025,
Accepted 11th May 2025

DOI: 10.1039/d5ma00257e

rsc.li/materials-advances

The quest for sustainable packaging solutions has led to increased interest in biodegradable polymers. Sodium alginate, despite its biocompatibility and biodegradability, faces significant challenges in terms of mechanical strength and barrier properties. This study explores the potential of enhancing the properties of alginate films by incorporating cellulose nanofibers (CNFs) modified with 3-aminopropyl triethoxysilane (APTES), which has not been reported in the literature previously. The modification process introduces amino silane groups without altering the morphology of the nanocellulose, as evidenced by TEM. The reinforcement led to a significant increase in the tensile strength of the films from 1.27 MPa to 16.23 MPa and the surface hydrophobicity of the films from 42° to 83°. The results suggested that amino silane-modified cellulose nanofibers can be promising fillers to be incorporated into alginate polymer matrices to improve their mechanical properties and structural densification for packaging and coating applications.

1. Introduction

The extensive reliance on petroleum-based polymers like polyethylene, polypropylene, and polystyrene has sparked major environmental concerns. These plastics, which are non-biodegradable, contribute to climate change through greenhouse gas emissions and accumulate in ecosystems, causing pollution and endangering wildlife. As the negative impacts of these petroleum-based packaging keep on increasing, there is a need to increase the production and usage of biodegradable polymers, especially in the food packaging sector.[1] These biodegradable polymers provide several advantages over conventional packaging materials, including better food preservation, stability, adaptability, and environmental benefits.[2] Although biodegradable polymers have been established for some time, they only hold a very low percentage in the food packaging market.[3] Several renewable and biodegradable polymers have been studied in various fields to create more environmentally friendly materials. One such biodegradable polymer is alginate, which, despite its biodegradability and biocompatibility, has certain drawbacks that restrict its use as a biopolymer for versatile applications. Alginate films exhibit poor mechanical strength, making them unsuitable for high-stress applications.[4] Their high-water sensitivity causes structural instability in moist environments, and their limited thermal stability restricts processing at elevated temperatures.[5] Furthermore, alginate has poor barrier properties, allowing high permeability to gases and moisture, reducing its effectiveness in packaging.[6] Likewise, its ion sensitivity and pH dependency make it unstable under varying environmental conditions, affecting its performance in biomedical and industrial applications.[7] Incorporating fillers into the biopolymeric matrix is one way to improve its functionalities.[8] Such fillers include graphene oxide,[9] halloysite nanotubes,[10] silicon dioxide,[11] zinc oxide,[12] *etc.* Although these fillers have been shown to improve mechanical strength and barrier properties and impart antibacterial functionalities, the toxicity of inorganic fillers like graphene oxide raises concerns over its use in food contact materials.[13]

Organic nanofillers, such as nanocellulose and chitin nanocrystals, are renewable and non-toxic, and are a suitable choice to improve the tensile strength, elasticity, and toughness of polymeric films. They create a more uniform and denser matrix by forming strong interactions with the polymer chains, which enhances load transfer and mechanical stability and reduces the transmission of gases.[14,15] However, they are generally less effective than inorganic fillers in blocking gases or moisture due to their hydrophilic nature.[16] This can be overcome by the modification of the organic moieties by chemical modifications, such as treating them with fatty acids and silanizing agents[17,18] and biological and enzymatic modifications.[19–21]

[a] *School of Advanced Sciences (SAS), Vellore Institute of Technology (VIT), Vellore 632014, Tamil Nadu, India*
[b] *Centre for Biomaterials, Cellular and Molecular Theranostics (CBCMT), Vellore Institute of Technology (VIT), Vellore 632014, Tamil Nadu, India. E-mail: joseph.nathanael@vit.ac.in*

† Electronic supplementary information (ESI) available. See DOI: https://doi.org/10.1039/d5ma00257e

Although enzymatic modifications offer an eco-friendlier modification approach, the chemical method is still preferred for modifications as it is comparatively cost-effective. Anionic and cationic surface modifications are easily introduced to their polymeric backbone using various reagents such as TEMPO (2,2,6,6-tetramethylpiperidine-1-oxyl) and alkenyl succinic anhydride, and anionic surfactants such as sodium alkyl naphthalene sulfonate. Bianchi *et al.* introduced carboxyl groups ($-COO^-$) onto the CNF surface using TEMPO oxidation to produce CNF microspheres suitable for the delivery of fertilizers.[22]

Each modification technique offers unique advantages depending on their targeted applications. APTES functionalization stands out for its ability to introduce amino silane groups,[23] allowing for further conjugation and enhanced interactions in nanocomposites and biomaterials. TEMPO oxidation is preferred for improving water dispersibility,[24] while acetylation[25,26] and alkylation[27] are more suitable for hydrophobic applications. Selecting an appropriate modification strategy depends on the required surface properties and application demands.

To date, the properties of alginate films incorporated with APTES-modified nanocellulose have not been explored. This study investigates the influence of amino silane-modified cellulose nanofibers extracted from coir fibers on the properties of sodium alginate polymeric films. It was hypothesized that incorporating these modified nanofibers into sodium alginate films can enhance their mechanical strength, thermal stability, and barrier properties, which are crucial for various applications such as packaging and biomedical devices. The cellulose nanofibers were extracted from a series of chemical treatments, followed by modification with 3-aminopropyltriethoxysilane. The modification results in the introduction of hydrophobic alkyl chains and silanol groups and enhances hydrogen bonding and polarity. The unmodified and modified films were analyzed for their structural, surface, and thermal properties. The physico-mechanical, optical, and thermal stabilities of the films were also studied. The findings of this study provide insights into the potential of amino silane-modified nanocellulose in enhancing the properties of alginate films, thereby contributing to the development of sustainable and high-performance composite materials in the fields of materials science and sustainable packaging.

2. Materials and methods

2.1. Materials

Coir fibers were collected from a local coir industry in Vellore, Tamil Nadu, India, and were pulverized into a powder. Alginic acid sodium salt from brown algae (Sigma Aldrich), sodium hydroxide pellets (Emparta), sulfuric acid (Emplura), sodium hypochlorite (Avra), glycerol (Avra), phosphotungstic acid (Sigma Aldrich), calcium chloride (Avra), dialysis membrane (Himedia), 3-amino propyltriethoxysilane APTES (SRL), and Milli-Q water (18.2 Ω) were used without further purification for the extraction of nanocellulose and fabrication of the biocomposite films.

2.2. Experimental

2.2.1. Extraction of nanocellulose. The chemical treatment method is utilised for the extraction of nanocellulose, which comprises three major steps: alkaline treatment, bleaching and acid hydrolysis.[28,29] The coir fibers were washed and dried for 24 hours in an oven at 60 °C and were ground to a size of about 1.0 mm. Then, the dried coir fibers were treated with 2% w/v of NaOH for 16 hours at a constant temperature of 90 °C. Then the residues were collected after filtration and dried in an oven at 45 °C for 12 hours. The alkali-treated coir fibers were bleached with 5 wt% sodium hypochlorite (NaClO) until a white pulp was produced. The residues were washed with water until they reached neutral pH and dried for 24 hours at 60 °C. For acid hydrolysis, the bleached coir fibers were subjected to acid treatment using 50% v/v of sulphuric acid for about 30 minutes while maintaining a constant temperature of 45 °C. Hydrolysis was quenched by adding Milli-Q water and washed twice with the same. The suspension was dialysed against Milli-Q water for 3–4 days until neutral pH was reached. The suspension was sonicated for 30 minutes and freeze-dried. The freeze dried nanocellulose was used for further analyses. The extracted cellulose nanofibers are identified as CNFs.

2.2.2. Modification of nanocellulose. The modification of cellulose nanofibers was performed with modifications from a previously reported procedure.[13] Briefly, 5% w/v of APTES solution was prepared, and glacial acetic acid was added until the pH was reduced to 4. The cellulose nanofibers were added, and the suspension was stirred magnetically for 2 hours at room temperature. The suspension was centrifuged at 5000 rpm for 10 min, and the supernatant was discarded. For the modification, the precipitate was dried in a hot air circulating oven at 110 °C for 15 min. The modified cellulose nanofibers were washed with 95% ethanol to remove unreacted APTES and dried in an oven at 60 °C (Fig. 1). The modified cellulose nanofibers are identified as APCNFs.

2.2.3. Preparation of bio-composite films. For the filmogenic solution, sodium alginate solution (3% w/v) was prepared by dissolving the biopolymer in Milli-Q water at 60 °C under continuous stirring. Glycerol (0.5 mL/1 g of sodium alginate) and APCNFs with 5%, 10%, 15% and 20% w/w of sodium alginate were added to the filmogenic solution. The mixture was homogenized under 10 000 rpm to facilitate the dispersion of the APCNFs. The solutions were degassed using an ultrasonicator (40 Hz) (model and make). The filmogenic solution was cast onto a 150 mm Petri plate and dried in a hot air circulating oven at 45 °C. The films were peeled off, cross-linked using 2% w/v of $CaCl_2$ solution and dried at room temperature. The dried films were stored in a desiccator for further studies (Fig. 2).

2.3. Characterisation

Powder X-ray diffraction (XRD) analysis was performed using a Bruker D8 advance diffractometer equipped with a Lynx eye detector, monochromated with Cu-Kα radiation (λ = 1.54 Å) in the 2θ range of 10–90. The crystallinity index (CI%) of the CNFs

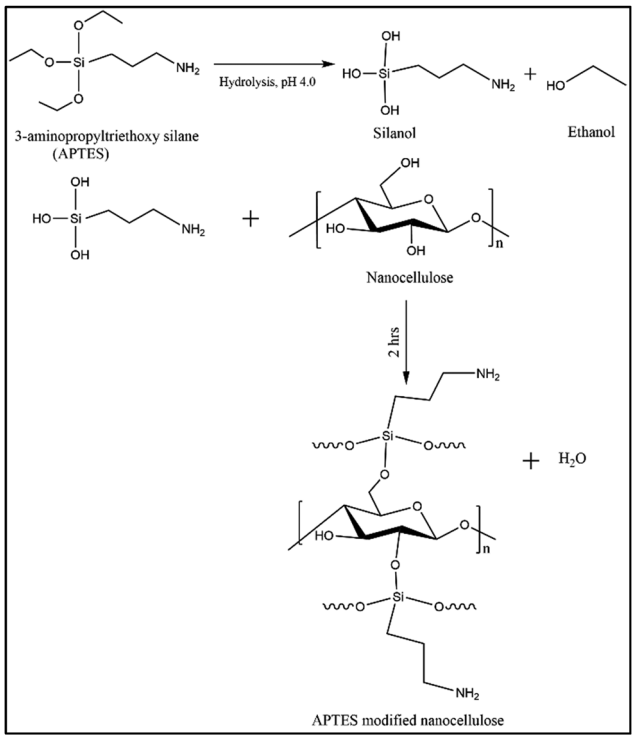

Fig. 1 Reaction scheme for the surface modification of nanocellulose with APTES.

was determined using the following formula:

$$\mathrm{CI}\,\% = \frac{I_c}{I_a} \times 100,$$

where I_c is the area of the crystalline region and I_a is the total area of amorphous and crystalline regions in the diffractogram.

The functional groups in the CNFs and the interactions in the bio-composite films were assessed using an FT-IR Spectrometer (Thermo Fisher, USA, Model Nicolet iS50) in the spectral region of 4000–400 cm^{-1}. All the experiments were conducted in ATR mode with a scan rate of 64 scans per minute, and the spectra were recorded using OMNIC software. The morphological features of the extracted CNFs were investigated using transmission electron microscopy (TEM). The aqueous CNF suspension (0.1 wt%) was sonicated for 10 minutes, and 50 μL of the suspension was placed on the TEM grid, followed by staining with 2% phosphotungstic acid. The images were analyzed using ImageJ software. The alginate films without the addition of fillers and crosslinkers were used as the control. At five random locations, the thickness of the films was measured using a digital micrometer (Mitutoyo), and the readings were recorded by gradually reducing the micrometre gap until the first sign of contact. The purity, surface composition, and functionalization of the CNF and APCNF were investigated using XPS (ULVAC-PHI VersaProbe 4). The surface-wetting characteristics of the bio-composite films were analyzed using a contact angle meter (HOLMARC: Model: HO-IAD-CAM-01A) by the sessile drop method. Five microliters of Milli-Q water were deposited on the films, and the contacting and receding angles obtained during the first 60 seconds after deposition were recorded. The measurements were performed in triplicate. To assess the mechanical properties of the bio-composite film, the tensile strength, tensile modulus, and elongation at break were measured using a universal tensile machine (Model HK10 Tinius Olsen, USA) according to ASTM D882-18. The films were cut into 15 mm×120 mm strips, and the average thickness of each strip was measured. A load cell of 500 N was used; the gauge length of the films was kept at 100 mm, and the strain rate was kept at 10 mm min^{-1}. Three measurements were taken for each sample, and the average value was calculated. The thermal stabilities of the CNF and APCNF and the bio-composite films were analyzed using a thermogravimetric analyzer (TA Instruments, USA, Model SDT Q600) in the temperature range of 25 °C to 800 °C with a heating rate of 20 °C min^{-1}. The tests were conducted

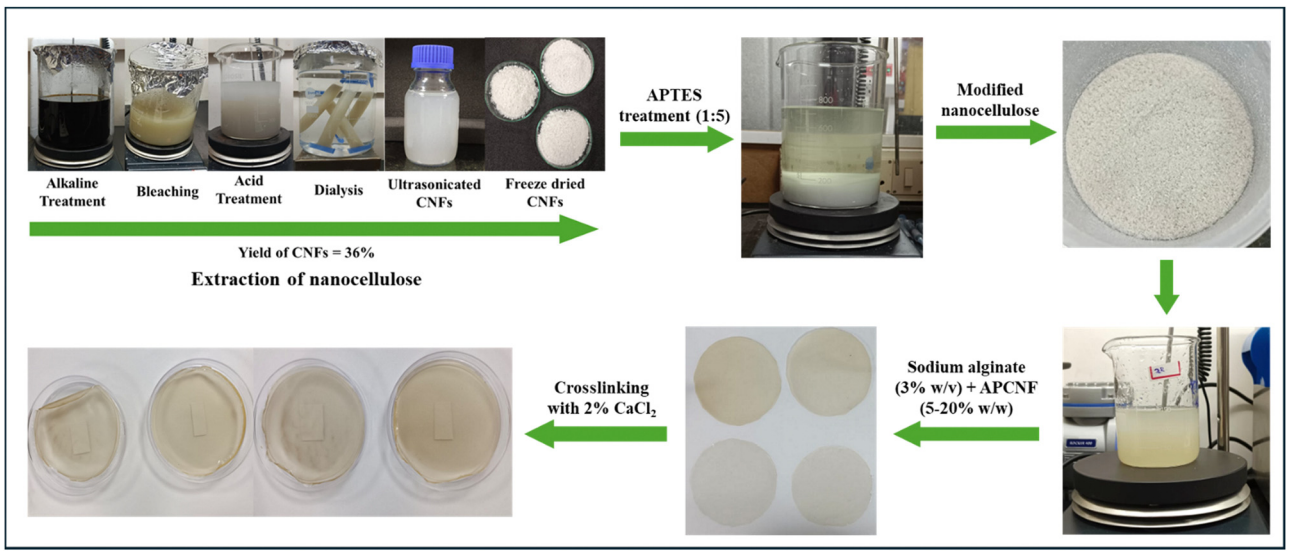

Fig. 2 Fabrication of APCNF-incorporated alginate films.

under a nitrogen atmosphere (20 mL min^{-1}). The opacity of the films was analyzed using a UV-vis spectrophotometer. The films were cut into 2 cm × 4 cm rectangular strips, and their absorbance at 600 nm was recorded. The opacity of the films was calculated using the following formula:

$$\text{Opacity} = \frac{\text{Abs}_{600}}{x},$$

where Abs_{600} is the absorbance of the film at 600 nm and x is the thickness of the film in millimeters. Films were digitally photographed, and the color was analyzed using a dedicated app (ColorAnlz). The film's color values (ΔE) were calculated using the following formula:

$$\Delta E = \sqrt{\Delta L^2 + \Delta a^2 + \Delta b^2},$$

where L is the brightness/darkness value, a is the redness/greenness value, and b is the yellowness/blueness value. Alginate films without crosslinkers and fillers were used as a control as crosslinked alginate films without the addition of fillers had fractures after drying.[30] All the experiments were performed in triplicate, and one-way ANOVA analysis was performed for statistical analysis.

3. Results and discussion

3.1. Extraction and modification of cellulose nanofibers

3.1.1. Structural and chemical composition analysis. FT-IR was used to identify the organic functional groups present in the raw coir, alkaline-treated, bleached coir, and acid-hydrolysed coir fibers. Fig. 3(a) shows the FTIR spectrum obtained after each treatment process. Peaks at around 3342 cm^{-1} and 1026 cm^{-1} were observed in all the samples. The peak at around 3342 cm^{-1} corresponds to the stretching of the –OH group, while the peak at around 1026 cm^{-1} indicates the asymmetric stretching of the C–O–C link, a characteristic of polysaccharides. The intensity of both the peaks increases after the treatment processes, implying an increase in the cellulose content and its purity, which is also observed in other studies.[31,32] In the alkali-treated fibers, a few peaks with low intensity are present at around 1722 cm^{-1} and 1504 cm^{-1}, which are attributed to the presence of aromatic groups in lignin, indicating that lignin is not completely removed after the alkaline treatment. The peaks between 2900 cm^{-1} and 2920 cm^{-1} are distinct in the bleached and acid treated samples, and they denote the C–H stretching vibration corresponding to methylene groups of the polysaccharide. Also, the characteristic β-1,4 glycosidic bond of cellulose is observed in the bleached and acid hydrolysed samples at around 898 cm^{-1}. In the final acid-treated and dialysed fibers, there is an absence of peaks at 1722 cm^{-1} and 1504 cm^{-1}, which implies the complete removal of lignin[33] (Fig. 3(a)). After APTES treatment, a new peak at 1562 cm^{-1} was observed in the spectrum, which is assigned to the NH bending of the amine groups in APTES (Fig. 3(b)). The bonds corresponding to Si–O–C and Si–O–Si were not observed in the FTIR spectra due to the possible overlap from strong vibrations from the C–O–C bonds of

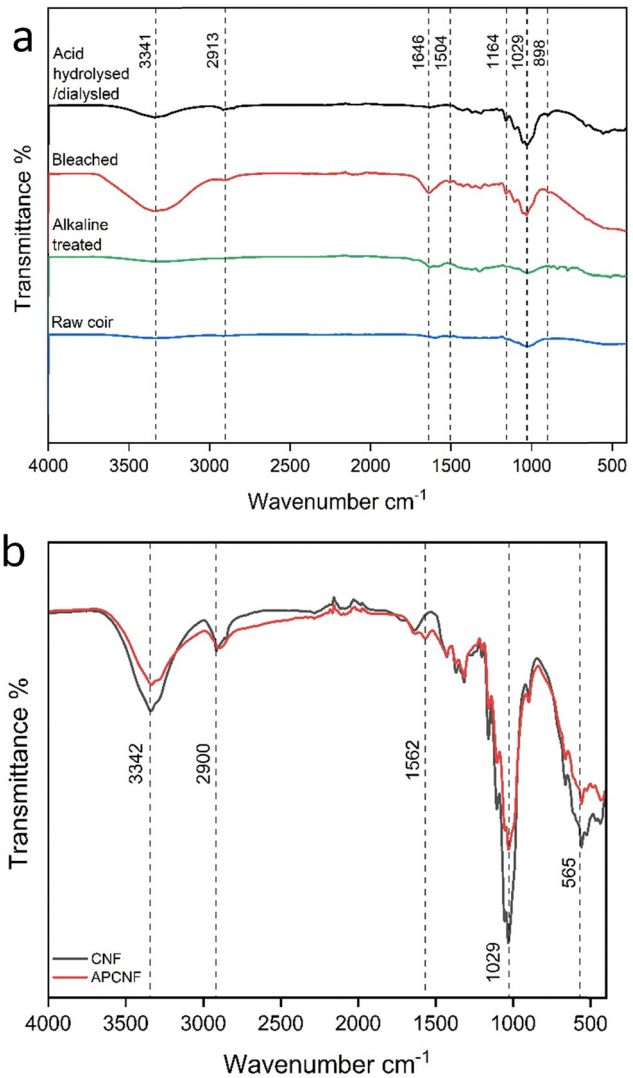

Fig. 3 (a) FTIR spectra after each treatment process of nanocellulose extraction. (b) FTIR spectra of APCNF.

cellulose in the spectral region of 1100–900 cm^{-1}.[30] The other functional groups corresponding to the spectral regions are tabulated in the ESI† (Tables S1 and S2).

In the XRD diffractograms, broad peaks were found in (Fig. 4 (a)) raw coir and alkaline-treated coir fibers, whereas bleached and acid hydrolyzed coir displayed narrow peaks at $2\theta = 16.32°$, depicting an improved crystallinity.[31] The broad peaks in the diffractograms of untreated coir fibers and alkali-treated fibers were due to the presence of amorphous lignin and hemicellulose. After treatment with alkali and subsequent bleaching, they were removed and during the acid treatment, the amorphous regions of cellulose were hydrolysed leaving behind the crystalline cellulose (Table S3, ESI†). The hydrolytic cleavage of the glycosidic bonds in cellulose occurs during the acid treatment which leaves individual crystallites, causing a marked improvement in crystallinity.[32] The obtained pattern of the acid-hydrolyzed cellulose nanofiber is in accordance with the ICDD pattern for cellulose (ICDD 50-2241). No polymorphic

transition between the cellulose types was observed after the alkaline treatment as a low concentration of alkali was used (2 wt%).[33] Major diffraction peaks were observed at 16.32° and 22.12°, which corresponds to the planes (110) and (200), respectively, indicating a cellulose type-I crystal structure.[34–36] The diffractograms before (Fig. 4(b)) and after modification (Fig. 4(c)) showed no significant difference, and the crystallinity index of the CNFs was found to be 63%. After modification (Fig. 4(b)), there is a slight decrease in the crystallinity (C.I = 57%) of the nanofibers, which can be accounted for due to the attachment of silane groups onto the cellulose nanofibers. This shows that the modification has only occurred on the surface of the cellulose nanofibers and does not change the crystal structure of the nanocellulose.[37,38] However, a slight broadening of the peak at 2θ = 16.32° in the APCNF denotes the increase in amorphous nature, which can be attributed to the grafting of amino-silane moieties on the cellulose nanofiber.

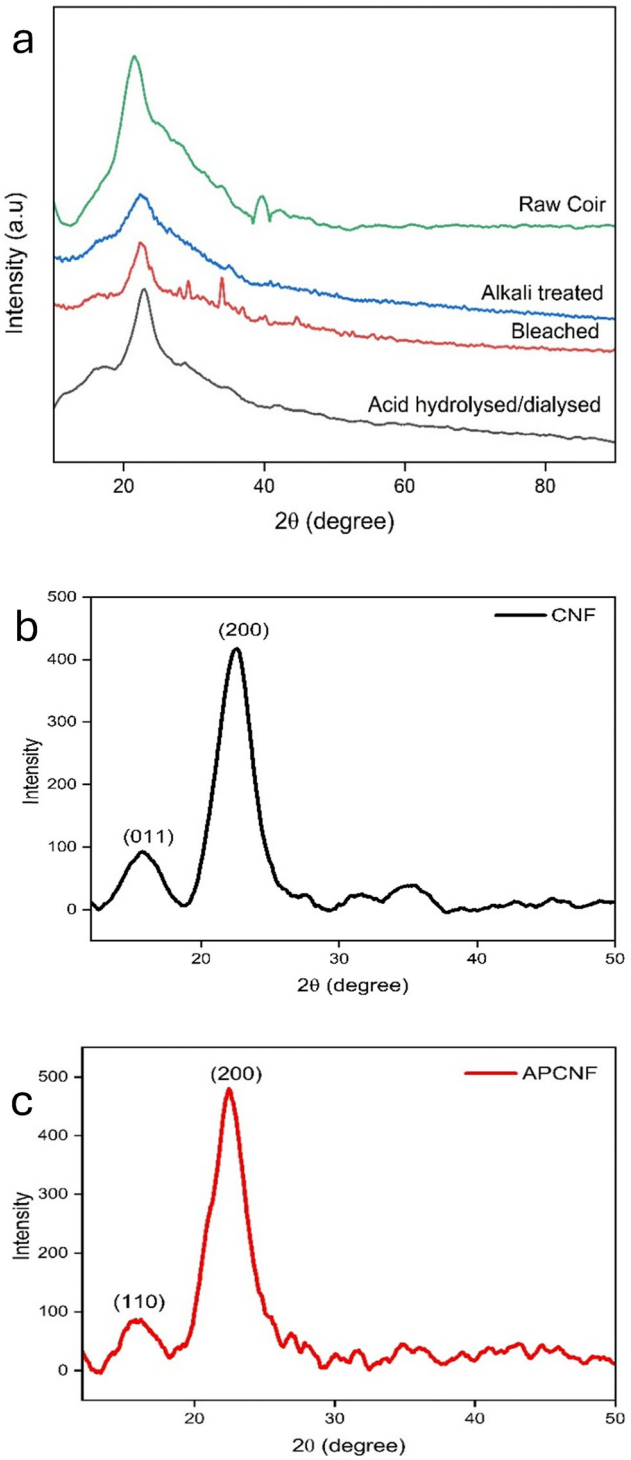

Fig. 4 (a) XRD diffractogram after each treatment process for the extraction of nanocellulose. XRD diffractogram of (b) CNF cellulose and (c) APCNF.

3.1.2. Elemental composition. The elemental composition of the CNF and APCNF was further studied using XPS (Fig. 5(a) and (b)). The peaks at 532.8 and 286.5 eV in the XPS spectrum of the CNF (Fig. 4(a)) confirmed the presence of oxygen (O 1s) and carbon atoms (C 1s). The spectrum also showed trace amounts of Na and Cl atoms, which is due to the remnants from the bleaching process. After APTES modification (Fig. 5(b)), new peaks were observed at 400 and 102 eV, which are associated

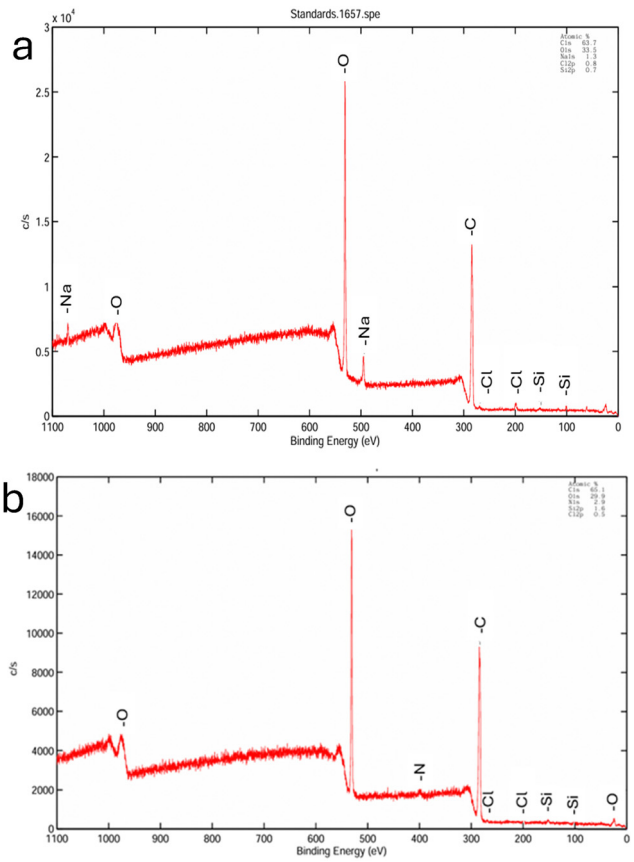

Fig. 5 XPS survey scan of (a) CNF and (b) APCNF.

Table 1 Atomic concentration of the CNF and APCNF

Atomic (%)	C 1s	O 1s	Si 2p	N 1s
CNF	63.7	33.5	0. 7	0.0
APCNF	65.1	29.9	1.6	2.9

with N 1s and Si 2p.[39] Several studies have reported the presence of silica in coconut husk ash,[40–42] which explains its occurrence in the survey spectrum of CNF. The atomic concentrations of the nanofibers before and after modification with APTES are given in Table 1. The APCNF showed the presence of nitrogen, constituting about 2.9%. An increase in the carbon composition was observed from 63.7% to 65.1%, and silicon constituted about 1.6% of the APCNF, indicating that a chemical bond is formed between nanocellulose and APTES. The change in the atomic percentage of CNF and APCNF in the survey spectrum confirms the successful grafting of the amino silane chain onto the cellulose nanofibers. The elemental composition of the APCNF is in agreement with the previously reported study.[43]

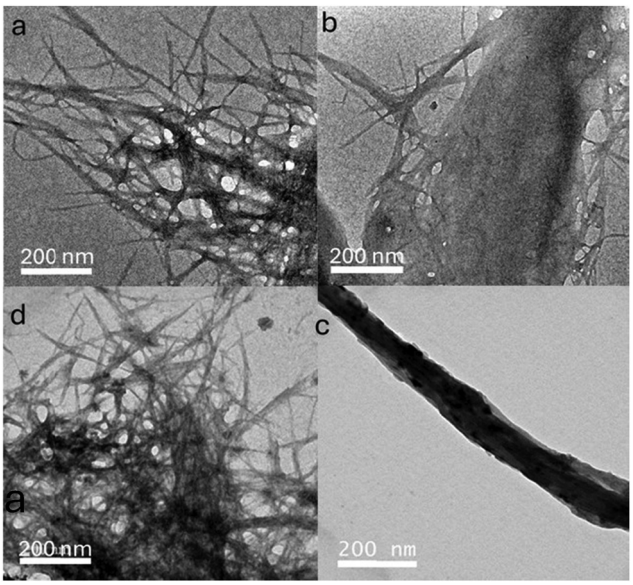

Fig. 6 TEM images (scale: 200 nm) of (a) and (b) CNF and (c) and (d) APCNF.

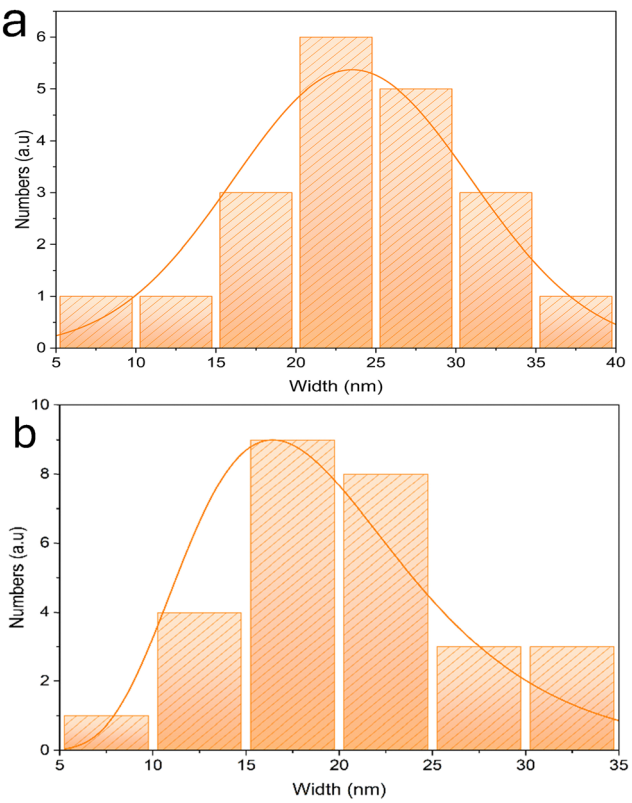

Fig. 7 Distribution plot of (a) CNF and (b) APCNF.

3.1.3. Morphology. TEM analysis (Fig. 6) confirmed the fiber-like morphology of the CNF and APCNF. Aggregation of the fibers was observed in the CNF and APCNF. The average width of the CNF is 23.5 nm (Fig. 7(a)), and that of the APCNF is 16.41 nm (Fig. 7(b)). This indicates that the modification process has not caused any significant changes in the morphology or size of the nanofibers. Similar observations were reported by other researchers where APTES treatment did not affect the morphology of the cellulose nanocrystals.[38,43]

3.1.4. Thermal properties. The thermal stability of the CNF and APCNF was inspected using TGA (Fig. 8(a)) and DTA

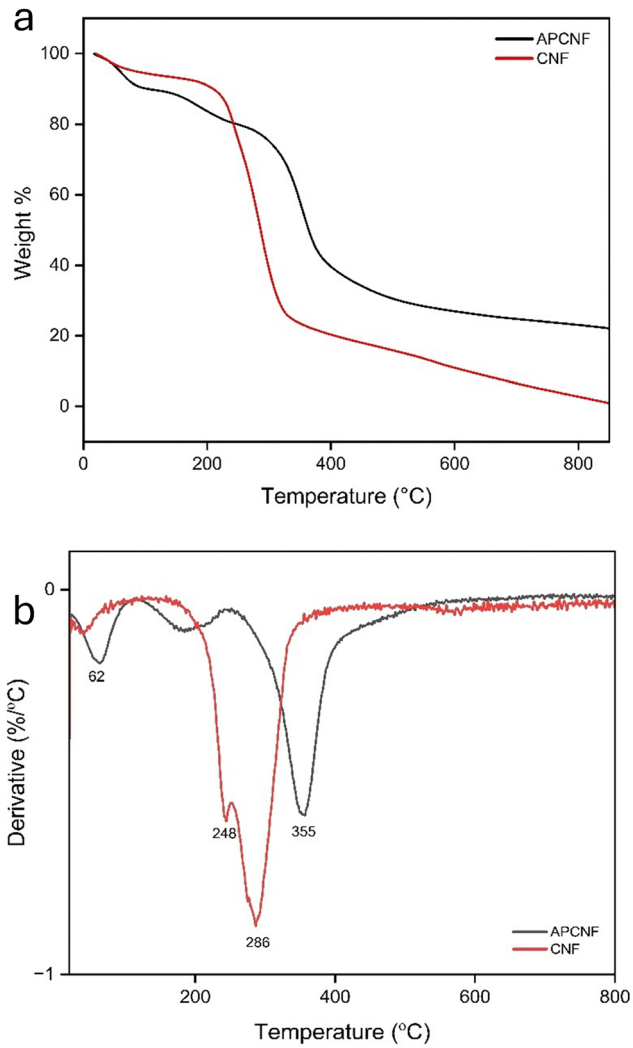

Fig. 8 TGA thermograms of (a) CNF and APCNF and (b) DTG curves of CNF and APCNF.

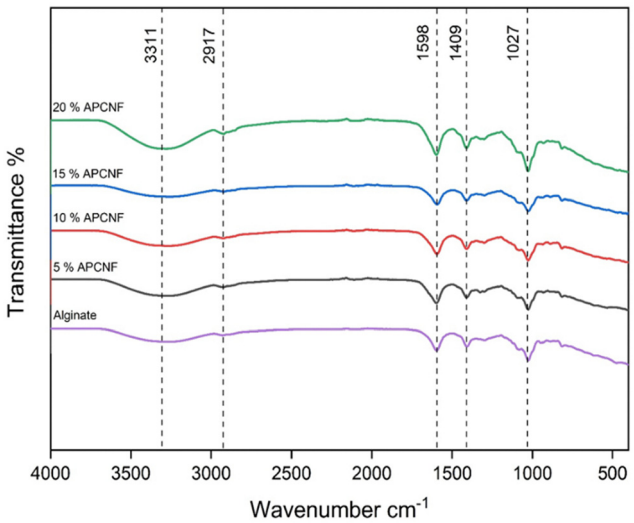

Fig. 9 FTIR spectra of the APCNF incorporated films.

(Fig. 6(b)). An initial weight loss due to surface-bound moisture was observed in the CNF and APCNF (Fig. 8(a)), followed by the onset of degradation of the nanofibers. The degradation of the CNF started at 243 °C, while that of the APCNF occurred after 300 °C. This can be explained by the grafting of amino-silane groups to the cellulose backbone. The increase in the carbonaceous content and the presence of silicon have brought down the onset of degradation of the APCNF. This is also evident from the DTG curves (Fig. 8(b)), where the maximum degradation temperature of the CNF is 286 °C and that of the APCNF is 355 °C.

3.2. Properties of APCNF-reinforced alginate films

3.2.1. Structural characterization and chemical composition. FTIR analysis (Fig. 9) showed the characteristic OH stretching in all the films at 3311 cm^{-1}. The CH stretch of the methylene groups in alginate and amino silane groups and that of cellulose were found at 2917 cm^{-1}. However, the intensity of the OH stretching was high in the film with a filler concentration of 20% compared to the others with a lower concentration. The bands at 1409 cm^{-1} and 1027 cm^{-1} correspond to the stretching of carboxylate groups in the pure alginate film and the APCNF loaded films (Table S4, ESI†). The intensity of the OH group increased with the increase in the filler content and was highest for the 20% APCNF incorporated film.

3.2.2. Morphology

3.2.2.1. SEM. The morphological features of the APCNF-incorporated alginate films were analysed using SEM (Fig. 10). The control alginate film showed a smooth morphology (Fig. 10(a)), while the APCNF-incorporated films displayed a granule-like surface morphology. In 10% APCNF (Fig. 10(c)), an even distribution of the granules can be observed, while in 15% APCNF (Fig. 10(d)), the granules are larger and compact with an inhomogeneous distribution. Native CNFs carry negative charges on their surfaces because of the hydroxyl groups they contain. When CNFs undergo surface modification with APTES, positively charged amino groups are added to their surface. In an aqueous environment, these positive charges can interact with the negatively charged CNFs, which can promote aggregation of the fibers and also increase surface roughness.[44] The biocomposite film with the highest APCNF content (Fig. 10(e)) exhibited an overlapped layer-like structure, indicating an aggregation between the fillers.

3.2.3. Surface hydrophobicity and physico-mechanical properties

3.2.3.1. Contact angle. The surface hydrophobicity of a polymer film was measured using a contact angle goniometer. The surface hydrophobicity of the alginate composites increased with the increase in the filler content ($P < 0.05$). The pure alginate film exhibits a water contact angle of 42°, while the films with APCNF as a filler at higher concentrations (20 w/w%)

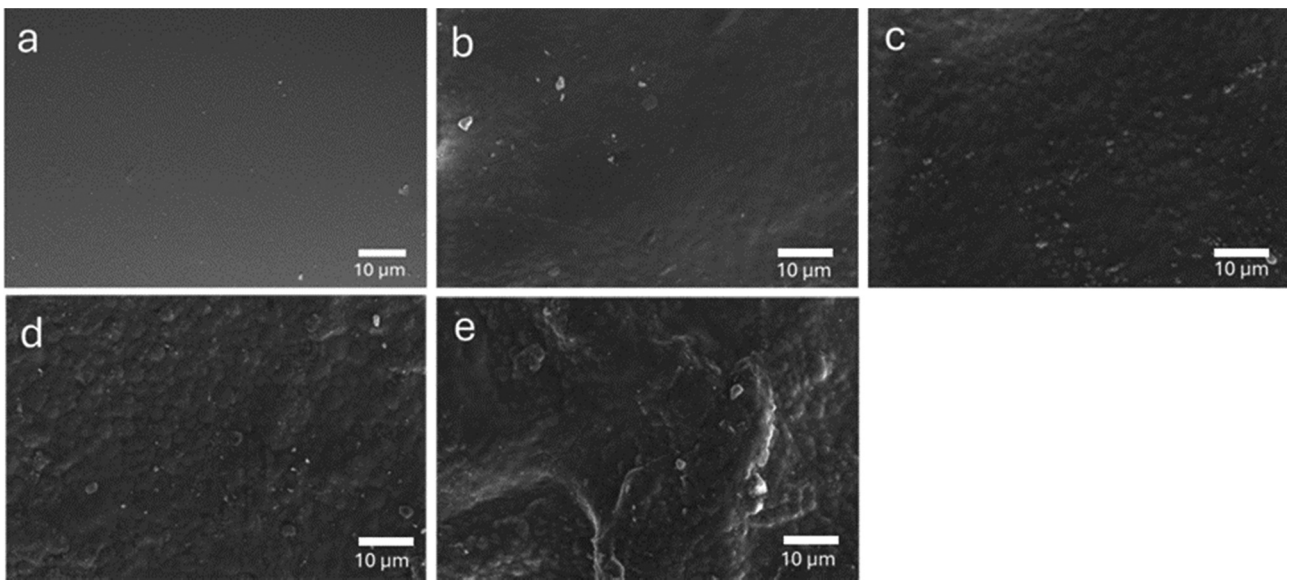

Fig. 10 Morphological features of the films (scale: 10 μm): (a) pure alginate, (b) 5% APCNF, (c) 10% APCNF, (d) 15% APCNF, and (e) 20% APCNF.

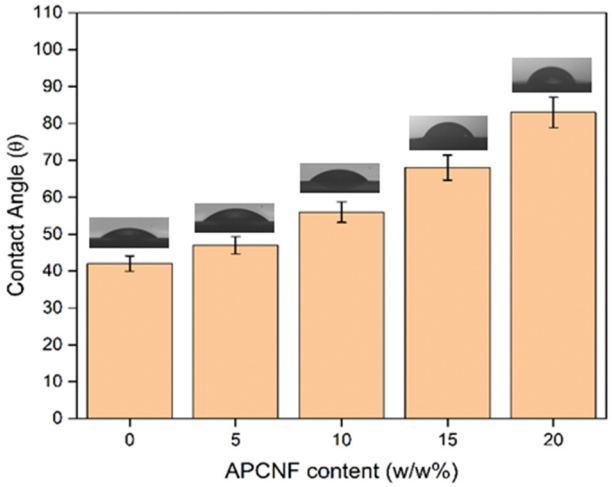

Fig. 11 Contact angle of APCNF-incorporated alginate films.

reached a water contact angle of up to 83° (Fig. 11). Nanocelluloses are rich in hydroxyl groups, which impart hydrophilicity to them. As observed in ref. 45, the increasing nanocellulose concentration can decrease the water contact angle, making them more hydrophilic. Modification of nanocellulose with APTES causes the hydrophobic alkyl chains to orient themselves along the surface.[13,46] The increase in the water contact angle can be attributed to the hydrophobic nature of the APCNF. The silane groups along with the grafting of the alkyl groups have imparted hydrophobicity, and the incorporation of APCNF as a filler in the alginate polymer has caused structural densification of the films and increased surface roughness, as observed in SEM (Fig. 10), thereby decreasing porosity and enhancing water holding capacity.[47] The obtained results are in close agreement with previous studies.[48]

3.2.3.2. Tensile strength. The mechanical properties of the alginate-APCNF bio-composite films are shown in Fig. 12(a) and (b)

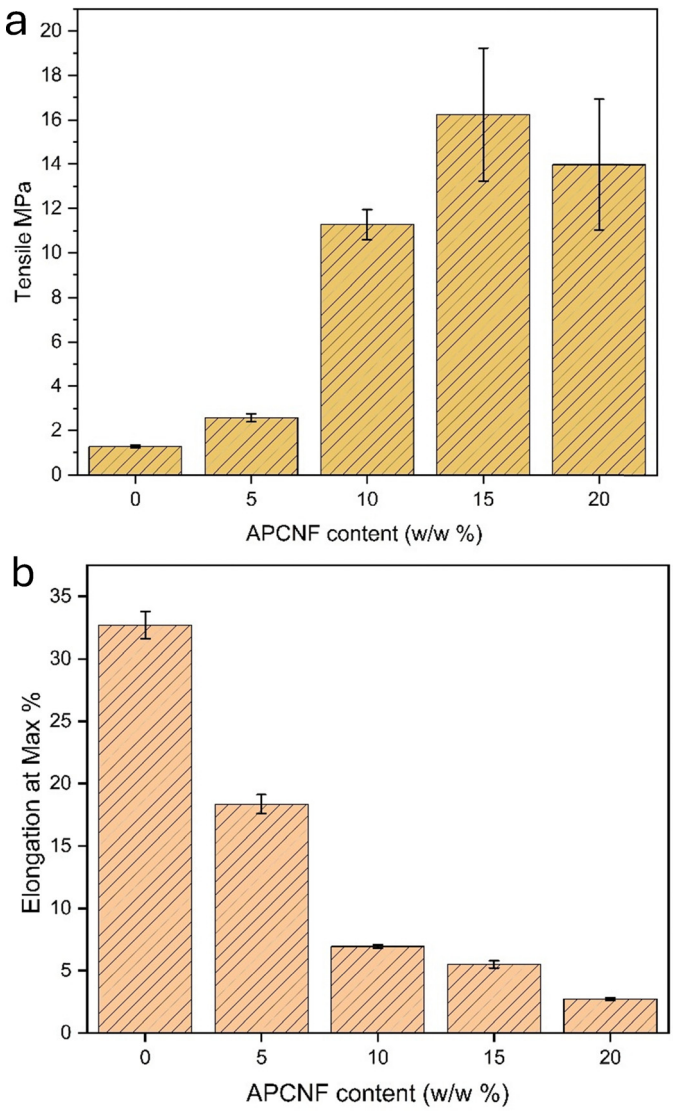

Fig. 12 (a) Tensile strength and (b) percentage elongation of APCNF-incorporated alginate films.

Table 2 Tensile strength and percentage elongation

Film	Tensile (MPa)	Elongation at max%	Thickness (mm)
0%	1.27 ± 0.06	32.25 ± 1.08	0.112 ± 0.06
5% APCNF	2.57 ± 1.91	17.79 ± 0.76	0.181 ± 0.04
10% APCNF	11.27 ± 0.68	6.9 ± 1.3	0.200 ± 0.03
15% APCNF	16.23 ± 3.14	5.42 ± 0.2	0.225 ± 0.07
20% APCNF	13.98 ± 2.9	2.73 ± 0.12	0.252 ± 0.07

Each value is a mean of triplicates with the standard deviation. Any two values in the same column are significant ($p > 0.05$).

and Table 2 ($P < 0.05$). The tensile strength of the film increased with incorporation of APCNF up to 15 w/w%, which displayed a strength of 16.23 MPa, but on further increasing the concentration, the tensile strength reduced to 13.9 MPa. Higher amounts of silane loading must have promoted the agglomeration of fibers, negatively affecting dispersion, thus leading to low mechanical strength and flexibility. The surface morphology (Fig. 10) of the films supports the aggregation of the fillers at a higher concentration, with 20% loading causing an overlapped layer-like morphology. The percentage elongation at break showed a steep decrease with increased concentrations of APCNF (Fig. 12(b)). Tanzina *et al.* incorporated nanocellulose as a filler for the alginate matrix, and the percentage elongation decreased from 10 to 5% when the concentration of the filler was from 1 to 8 w/w% of the dry matrix.[49]

3.2.4. Thermal properties. Thermal degradation of the films was inspected using TGA (Fig. 13(a)) and DTA (Fig. 13(b)). The degradation comprised four steps in all the films, with an initial loss of moisture around 56–100 °C. The second degradation started at around 220–260 °C due to the thermal degradation of glycerol. At around 320–400 °C, decomposition of the APCNF occurs, and the films with higher concentrations exhibit an increased thermal stability compared to lower concentrations, indicating that the incorporation of APCNF slows down the decomposition process. In the 5% APCNF, the initial degradation occurred at 199 °C, 50% of the degradation occurred at 245 °C, and 12.08% of carbonaceous mass remained at the end of the decomposition process. In the 10% APCNF, the film attains a maximum degradation at 270 °C, and the other two films with a higher APCNF content also exhibit a maximum degradation temperature of 270 °C. The addition of the APCNF as a filler has shifted the degradation to higher temperatures, suggesting better thermal stability of APCNF-reinforced films, which also indicated strong interactions between the APCNF and the alginate matrix. The lowest residues were exhibited by 15% loading of APCNF, and 10% loaded films exhibited the highest remaining residue. In a study involving APTES modification of cellulose nanocrystals, the amino-silane surface modification reportedly increased the thermal stability of PVA.[38]

3.2.5. Optical properties

3.2.5.1. Colour and opacity. The color of a film is important when it comes to packaging applications as visual appearance influences the consumer's acceptance of the product.[50] Next to transmittance, opacity is the parameter that is used to determine the transparency of a material.[51] Fig. 14 shows the visual appearance of the films, and Table 3 shows the CIE LAB values of color coordinates, L^*, a^*, b^*, and total difference (ΔE). All the

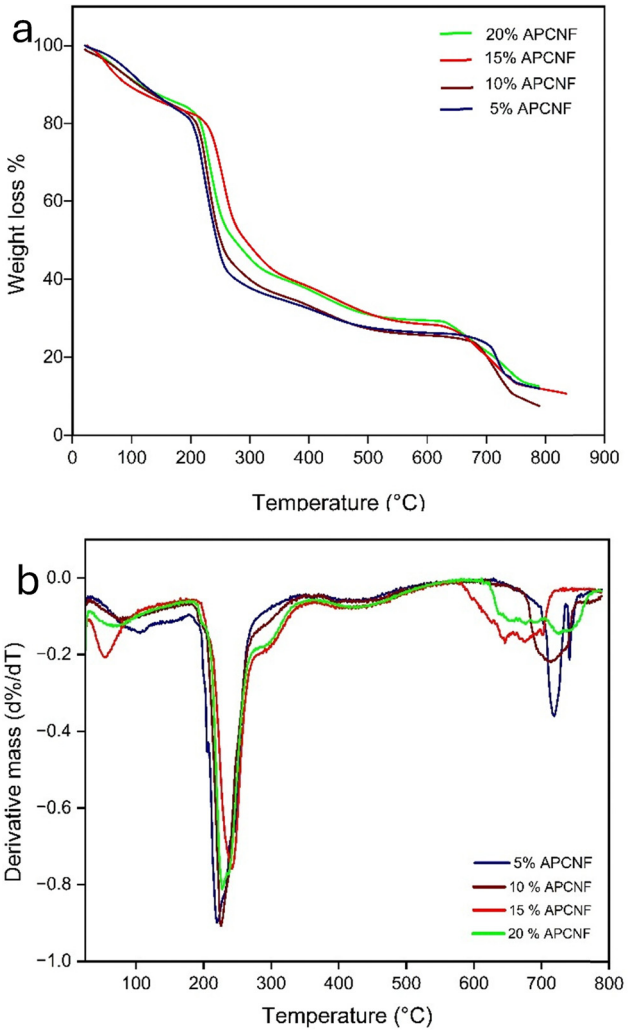

Fig. 13 (a) DSC thermograms of APCNF-incorporated alginate films and (b) DTG curves of APCNF-incorporated alginate films.

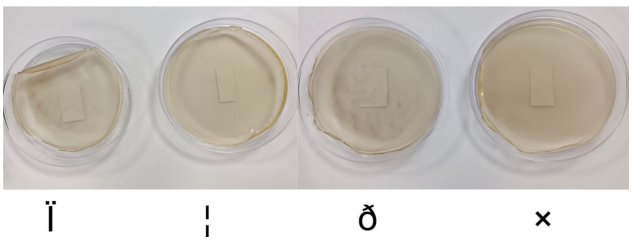

Fig. 14 Visual appearance of APCNF-incorporated alginate films: (a) 5% APCNF, (b) 10% APCNF, (c) 15% APCNF, and (d) 20% APCNF.

films are pale yellow in color, and the yellowness index increases in correspondence with the presence of the APCNF in them. The lightness index is increased at higher concentrations of APCNF as the light gets scattered by the APCNF particles, reducing the transparency of the films. This is further evidenced by the absorption of the films at 600 nm (Table 4) ($P < 0.05$). The pure alginate film is nearly transparent compared to the films incorporated with APCNF. However, the decrease in the film's lightness may

Table 3 CIE LAB values of the films

Film	L	a	b	ΔE
APCNF 5%	57.9	0.5	10.9	39.54
APCNF 10%	62.2	0.3	15.6	37.1
APCNF 15%	61.7	0.5	19.2	39.16
APCNF 20%	55.7	0.9	27.5	48.62

Table 4 Opacity of the films

Film	Absorbance	Thickness (mm)	Opacity
Pure alginate	0.0883	0.112 ± 0.06	0.78 ± 0.15
5% APCNF	0.8966	0.181 ± 0.04	4.953 ± 0.13
10% APCNF	1.1968	0.200 ± 0.03	5.984 ± 0.12
15% APCNF	1.4324	0.225 ± 0.07	6.366 ± 0.07
20% APCNF	1.6667	0.252 ± 0.07	6.6 ± 0.1

Each value in the second and third columns is a mean of triplicates with the standard deviation. Any two values in the same column are significant ($p > 0.05$).

help avoid oxidative deterioration in packaged foods caused by exposure to visible and ultraviolet light, leading to nutrient losses, discoloration, and off-flavors.[36]

4. Conclusion

In the present study, biocomposite films comprising alginate and amino silane-modified cellulose nanofibers was fabricated and their physico-chemical and mechanical properties were evaluated. The nanofibers were extracted from coir fibers using chemical treatment, and amino-silane groups were introduced into the nanocellulose by treating them with APTES. The CNF and APCNF were characterized by XRD, FTIR, TEM, and XPS. The modification did not cause any significant changes in the morphology of the nanocellulose, and the modification occurred only on the surface of the cellulosenano fibers. The APCNFs were incorporated at different concentrations into the alginate polymeric matrix, and the resulting biocomposites were translucent with an increased surface hydrophobicity and mechanical strength. Also, higher concentrations of APCNF incorporation tend to slow down the decomposition of the biocomposite film. The alginate-APCNF composites can be used in biodegradable packaging and bio-based coating materials. Further studies on the permeability of the biocomposite film are to be performed to study the influence of the APCNF as a filler in enhancing the barrier properties of alginate polymeric materials.

Author contributions

S. A. and A. J. N. contributed to conceptualization; S. A. contributed to writing – original draft preparation; A. J. N. contributed to review, editing, and supervision.

Data availability

Any additional data from this work are available from the corresponding author upon reasonable request.

Conflicts of interest

The authors declare no conflict of interest.

Acknowledgements

A. J. N. would like to acknowledge the financial support from the Department of Biotechnology, Government of India, through the Ramalingaswami Re-entry fellowship (D.O. No. BT/HRD/35/02/2006) and VIT faculty startup SEED grant. S. A. and A. J. N. thank TEM, XPS and other instrumentation facilities from VIT for characterisation studies.

References

1 S. Mangaraj, A. Yadav, L. M. Bal, S. K. Dash and N. K. Mahanti, Application of Biodegradable Polymers in Food Packaging Industry: A Comprehensive Review, *J. Packag. Technol. Res.*, 2019, **3**(1), 77–96, DOI: **10.1007/s41783-018-0049-y**.

2 Y. Zhong, P. Godwin, Y. Jin and H. Xiao, Biodegradable polymers and green-based antimicrobial packaging materials: A mini-review, *Adv. Ind. Eng. Polym. Res.*, 2020, **3**(1), 27–35, DOI: **10.1016/j.aiepr.2019.11.002**.

3 C. L. Reichert, *et al.*, Bio-Based Packaging: Materials, Modifications, Industrial Applications and Sustainability, *Polymers*, 2020, **12**(7), 7, DOI: **10.3390/polym12071558**.

4 D. R. Sahoo and T. Biswal, Alginate and its application to tissue engineering, *SN Appl. Sci.*, 2021, **3**(1), 30, DOI: **10.1007/s42452-020-04096-w**.

5 A. Mihaly Cozmuta, *et al.*, Thermal stability and *in vitro* digestion of alginate–starch–iron beads for oral delivery of iron, *Food Hydrocolloids*, 2023, **142**, 108808, DOI: **10.1016/j.foodhyd.2023.108808**.

6 R. Gheorghita Puscaselu, A. Lobiuc, M. Dimian and M. Covasa, Alginate: From Food Industry to Biomedical Applications and Management of Metabolic Disorders, *Polymers*, 2020, **12**(10), 10, DOI: **10.3390/polym12102417**.

7 A. Bibi, S. Rehman and A. Yaseen, Alginate-nanoparticles composites: kinds, reactions and applications, *Mater. Res. Express*, 2019, **6**(9), 092001, DOI: **10.1088/2053-1591/ab2016**.

8 J.-W. Rhim and P. K. W. Ng, Natural Biopolymer-Based Nanocomposite Films for Packaging Applications, *Crit. Rev. Food Sci. Nutr.*, 2007, **47**(4), 411–433, DOI: **10.1080/10408390600846366**.

9 S. Liu, Y. Li and L. Li, Enhanced stability and mechanical strength of sodium alginate composite films, *Carbohydr. Polym.*, 2017, **160**, 62–70, DOI: **10.1016/j.carbpol.2016.12.048**.

10 S. Kouser, *et al.*, Effects of reinforcement of sodium alginate functionalized halloysite clay nanotubes on thermo-mechanical properties and biocompatibility of poly (vinyl alcohol) nanocomposites, *J. Mech. Behav. Biomed. Mater.*, 2021, **118**, 104441, DOI: **10.1016/j.jmbbm.2021.104441**.

11 M. Yang, *et al.*, Preparation and property investigation of crosslinked alginate/silicon dioxide nanocomposite films,

J. Appl. Polym. Sci., 2016, **133**(22), 43489, DOI: **10.1002/app.43489**.

12 A. Akbar and A. K. Anal, Zinc oxide nanoparticles loaded active packaging, a challenge study against *Salmonella typhimurium* and *Staphylococcus aureus* in ready-to-eat poultry meat, *Food Control*, 2014, **38**, 88–95, DOI: **10.1016/j.foodcont.2013.09.065**.

13 H. Khanjanzadeh, *et al.*, Surface chemical functionalization of cellulose nanocrystals by 3-aminopropyltriethoxysilane, *Int. J. Biol. Macromol.*, 2018, **106**, 1288–1296, DOI: **10.1016/j.ijbiomac.2017.08.136**.

14 E. Jamróz, P. Kulawik and P. Kopel, The Effect of Nanofillers on the Functional Properties of Biopolymer-based Films: A Review, *Polymers*, 2019, **11**(4), 675, DOI: **10.3390/polym11040675**.

15 S. X. Tan, A. Andriyana, H. C. Ong, S. Lim, Y. L. Pang and G. C. Ngoh, A Comprehensive Review on the Emerging Roles of Nanofillers and Plasticizers towards Sustainable Starch-Based Bioplastic Fabrication, *Polymers*, 2022, **14**(4), 4, DOI: **10.3390/polym14040664**.

16 M. Hasan, *et al.*, Organic and inorganic fillers' role on the amelioration of Kappaphycus spp.-based biopolymer films' performance, *BioResources*, 2019, **14**(4), 9198–9213, DOI: **10.15376/biores.14.4.9198-9213**.

17 J. M. Morrissette, P. J. Carroll, I. S. Bayer, J. Qin, D. Waldroup and C. M. Megaridis, A methodology to produce eco-friendly superhydrophobic coatings produced from all-water-processed plant-based filler materials, *Green Chem.*, 2018, **20**(22), 5169–5178, DOI: **10.1039/C8GC02439A**.

18 S. S. Md Nor, M. F. Abdul Patah and M. Mat Salleh, Surface modification of bio-based composites via silane treatment: a short review, *J. Adhes. Sci. Technol.*, 2023, **37**(5), 801–816, DOI: **10.1080/01694243.2022.2049087**.

19 S. Sulaiman, M. N. Mokhtar, M. N. Naim, A. S. Baharuddin and A. Sulaiman, A Review: Potential Usage of Cellulose Nanofibers (CNF) for Enzyme Immobilization via Covalent Interactions, *Appl. Biochem. Biotechnol.*, 2015, **175**(4), 1817–1842, DOI: **10.1007/s12010-014-1417-x**.

20 H. Lu and Y. Tian, Nanostarch: Preparation, Modification, and Application in Pickering Emulsions, *J. Agric. Food Chem.*, 2021, **69**(25), 6929–6942, DOI: **10.1021/acs.jafc.1c01244**.

21 S. Afrin and Z. Karim, Isolation and Surface Modification of Nanocellulose: Necessity of Enzymes over Chemicals, *ChemBioEng Rev.*, 2017, **4**(5), 289–303, DOI: **10.1002/cben.201600001**.

22 S. Bianchi, D. França and R. Faez, Anionic and cationic cellulose nanofibrils as a macronutrient-carrying vehicle, *Cellulose*, 2024, **31**(2), 1053–1070, DOI: **10.1007/s10570-023-05662-2**.

23 R. Surkatti, *et al.*, Comparative analysis of amine-functionalized silica for direct air capture (DAC): Material characterization, performance, and thermodynamic efficiency, *Sep. Purif. Technol.*, 2025, **354**, 128641, DOI: **10.1016/j.seppur.2024.128641**.

24 T. Saito and A. Isogai, TEMPO-Mediated Oxidation of Native Cellulose. The Effect of Oxidation Conditions on Chemical and Crystal Structures of the Water-Insoluble Fractions, *Biomacromolecules*, 2004, **5**(5), 1983–1989, DOI: **10.1021/bm0497769**.

25 X. Zhang, *et al.*, Acetylated cellulose nanofibers enhanced bio-based polyesters derived from 10-undecanoic acid toward recyclable and degradable plastics, *Chem. Eng. J.*, 2024, **479**, 147797, DOI: **10.1016/j.cej.2023.147797**.

26 R. Sukmawan and M. W. Wildan, Optimizing Acetic Anhydride Amount for Improved Properties of Acetylated Cellulose Nanofibers from Sisal Fibers Using a High-Speed Blender, *ACS Omega*, 2023, **8**(30), 27117–27126, DOI: **10.1021/acsomega.3c02178**.

27 J. H. Lee, S. H. Park and S. H. Kim, Surface Alkylation of Cellulose Nanocrystals to Enhance Their Compatibility with Polylactide, *Polymers*, 2020, **12**(1), 1, DOI: **10.3390/polym12010178**.

28 K. Pavalaydon, H. Ramasawmy and D. Surroop, Comparative evaluation of cellulose nanocrystals from bagasse and coir agro-wastes for reinforcing PVA-based composites, *Environ. Dev. Sustainability*, 2022, **24**(8), 9963–9984, DOI: **10.1007/s10668-021-01852-9**.

29 K. M. F. Hasan, P. G. Horváth, S. Baş, Z. M. Mucsi, M. Bak and T. Alpár, Chapter 11 - Physicochemical and morphological properties of microcrystalline cellulose and nanocellulose extracted from coir fibers and its composites, in *Coir Fiber and its Composites*, ed. M. Jawaid, Woodhead Publishing Series in Composites Science and Engineering., Woodhead Publishing, 2022, pp. 255–273, DOI: **10.1016/B978-0-443-15186-6.00030-8**.

30 J. A. Sirviö, A. Kolehmainen, H. Liimatainen, J. Niinimäki and O. E. O. Hormi, Biocomposite cellulose-alginate films: Promising packaging materials, *Food Chem.*, 2014, **151**, 343–351, DOI: **10.1016/j.foodchem.2013.11.037**.

31 G. T. Melesse, F. G. Hone and M. A. Mekonnen, Extraction of Cellulose from Sugarcane Bagasse Optimization and Characterization, *Adv. Mater. Sci. Eng.*, 2022, **2022**(1), 1712207, DOI: **10.1155/2022/1712207**.

32 H. V. T. Luong, T. L. Le, X. H. Ly, T. P. Le, N. Y. Nguyen and D. T. Pham, Optimizing cellulose extraction from coconut coir pith via response surface methodology for improving methylene blue adsorption, *Int. J. Environ. Sci. Technol.*, 2025, **22**(7), 5591–5608, DOI: **10.1007/s13762-024-05963-4**.

33 N. Sharma, B. J. Allardyce, R. Rajkhowa and R. Agrawal, Rice straw-derived cellulose: a comparative study of various pretreatment technologies and its conversion to nanofibres, *Sci. Rep.*, 2023, **13**(1), 16327, DOI: **10.1038/s41598-023-43535-7**.

34 H.-M. Ng, *et al.*, Extraction of cellulose nanocrystals from plant sources for application as reinforcing agent in polymers, *Composites, Part B*, 2015, **75**, 176–200, DOI: **10.1016/j.compositesb.2015.01.008**.

35 A. Mittal, R. Katahira, M. E. Himmel and D. K. Johnson, Effects of alkaline or liquid-ammonia treatment on crystalline cellulose: changes in crystalline structure and effects on enzymatic digestibility, *Biotechnol. Biofuels*, 2011, **4**(1), 41, DOI: **10.1186/1754-6834-4-41**.

36 A. N. Vu, *et al.*, Cellulose nanocrystals extracted from rice husk using the formic/peroxyformic acid process: isolation and structural characterization, *RSC Adv.*, 2024, **14**(3), 2048–2060, DOI: **10.1039/D3RA06724F**.

37 L.-F. Wang, S. Shankar and J.-W. Rhim, Properties of alginate-based films reinforced with cellulose fibers and cellulose nanowhiskers isolated from mulberry pulp, *Food Hydrocolloids*, 2017, **63**, 201–208, DOI: **10.1016/j.foodhyd.2016.08.041**.

38 S. K. Amit, D. Gomez-Maldonado, T. Bish, M. S. Peresin and V. A. Davis, Properties of APTES-Modified CNC Films, *ACS Omega*, 2024, **9**(14), 16572–16580, DOI: **10.1021/acsomega.4c00439**.

39 M. N. A. M. Taib, T. S. Yee, D. Trache and M. Hazwan Hussin, Modification on nanocellulose extracted from kenaf (Hibiscus cannabinus) with 3-aminopropyltriethoxysilane for thermal stability in poly (vinyl alcohol) thin film composites, *Cellulose*, 2024, **31**(2), 997–1015, DOI: **10.1007/s10570-023-05671-1**.

40 W. Wang, Q. Bai, T. Liang, H. Bai and X. Liu, Preparation of amino-functionalized regenerated cellulose membranes with high catalytic activity, *Int. J. Biol. Macromol.*, 2017, **102**, 944–951, DOI: **10.1016/j.ijbiomac.2017.04.096**.

41 J. A. Y. Susanto, *et al.*, Twisted-chiral mesoporous silica from coconut husk waste designed for high-performance drug uptake and sustained release, *Microporous Mesoporous Mater.*, 2024, **367**, 112973, DOI: **10.1016/j.micromeso.2023.112973**.

42 M. F. Anuar, Y. W. Fen, M. H. M. Zaid, K. A. Matori and R. E. M. Khaidir, Synthesis and structural properties of coconut husk as potential silica source, *Results Phys.*, 2018, **11**, 1–4, DOI: **10.1016/j.rinp.2018.08.018**.

43 S. Barani, S. P. Sebastian, P. Dhevagi, M. Prasanthrajan and A. Suganthi, Synthesis of silica nanoparticles (SiNPs) from agro-wastes for removal of heavy metals from an aqueous medium – a mini review, *Green Chem. Lett. Rev.*, 2024, **17**(1), 2422416, DOI: **10.1080/17518253.2024.2422416**.

44 X. Tian, M. Wu, Z. Wang, J. Zhang and P. Lu, A high-stable soybean-oil-based epoxy acrylate emulsion stabilized by silanized nanocrystalline cellulose as a sustainable paper coating for enhanced water vapor barrier, *J. Colloid Interface Sci.*, 2022, **610**, 1043–1056, DOI: **10.1016/j.jcis.2021.11.149**.

45 O. T. Abafe Diejomaoh, *et al.*, Surface modification of cellulose nanomaterials with amine functionalized fluorinated ionic liquids for hydrophobicity and high thermal stability, *Carbohydr. Polym.*, 2024, **344**, 122519, DOI: **10.1016/j.carbpol.2024.122519**.

46 M. Ghasemlou, F. Daver, E. P. Ivanova, Y. Habibi and B. Adhikari, Surface modifications of nanocellulose: From synthesis to high-performance nanocomposites, *Prog. Polym. Sci.*, 2021, **119**, 101418, DOI: **10.1016/j.progpolymsci.2021.101418**.

47 M. Fernandes, *et al.*, Modification of Nanocellulose, in *Handbook of Biomass*, ed S. Thomas, M. Hosur, D. Pasquini and C. Jose Chirayil, Springer Nature, Singapore, 2023, pp. 1–39, DOI: **10.1007/978-981-19-6772-6_35-1**.

48 M. Ly and T. H. Mekonnen, Cationic surfactant modified cellulose nanocrystals for corrosion protective nanocomposite surface coatings, *J. Ind. Eng. Chem.*, 2020, **83**, 409–420, DOI: **10.1016/j.jiec.2019.12.014**.

49 T. Huq, *et al.*, Nanocrystalline cellulose (NCC) reinforced alginate based biodegradable nanocomposite film, *Carbohydr. Polym.*, 2012, **90**(4), 1757–1763, DOI: **10.1016/j.carbpol.2012.07.065**.

50 A. Mohamed and H. S. Ramaswamy, Characterization of Caseinate–Carboxymethyl Chitosan-Based Edible Films Formulated with and without Transglutaminase Enzyme, *J. Compos. Sci.*, 2022, **6**(7), 216, DOI: **10.3390/jcs6070216**.

51 S. Guzman-Puyol, J. J. Benítez and J. A. Heredia-Guerrero, Transparency of polymeric food packaging materials, *Food Res. Int.*, 2022, **161**, 111792, DOI: **10.1016/j.foodres.2022.111792**.